

Emergent Continuous Time Crystal in Dissipative Quantum Spin System without Driving

Shu Yang,¹ Zeqing Wang,^{3,2} Libin Fu,^{1,*} and Jianwen Jie^{2,†}

¹Graduate School of China Academy of Engineering Physics, Beijing 100193, China

²Shenzhen Key Laboratory of Ultraintense Laser and Advanced Material Technology, Center for Intense Laser Application Technology, and College of Engineering Physics, Shenzhen Technology University, Shenzhen 518118, China

³Department of Physics, Renmin University of China, Beijing 100872, China

(Dated: July 8, 2024)

Time crystal, a nonequilibrium phenomenon extending spontaneous symmetry breaking into the temporal dimension, holds fundamental significance in understanding quantum many-body physics. In this work, we explore the nonequilibrium phase diagram of a two-dimensional dissipative Heisenberg spin system without explicit coherent or incoherent external driving. We numerically identify the emergence of novel nonstationary oscillatory states by analyzing the spin dynamics. These states are categorized as limit cycle and chaos based on the Lyapunov exponent. Remarkably, the observed limit cycle behavior represents a continuous time crystal (CTC), spontaneously breaking the continuous time translation symmetry of the system. We further confirm those oscillatory behaviors by studying the stability against local perturbations applied to the system. Finally, we investigate the robustness of the emergent CTC by introducing isotropic Gaussian-type white noise into the interactions. This study provides many insights into the intricate interplay between the dissipation-induced spin downwards and anisotropic-interaction-induced spin precession or spin fluctuation, opening a new avenue for realizing dissipation-induced, heating-immune TCs.

Introduction.— Time crystal (TC) is originally proposed by Frank Wilczek to spontaneously break the time translation symmetry (TTS) in ground state or equilibrium state [1–4]. Although this idea were negated by a series of rigorous no-go theorems [5–7], ruling out TC in closed quantum systems with only short-range interactions [8], the introduction of time-dependent periodic coherent driving has enabled the realization of discrete TTS breaking [9–11]. This phenomenon, known as Floquet TC or discrete TC (DTC) [12–21], is characterized by subharmonic responses to the driving frequency and has been experimentally demonstrated in various systems [22–24] such as trapped-ions [25, 26] and superconducting qubits [27]. Its key challenge remains the heating-induced limited lifetime, despite mechanisms [26, 28–31] like many-body localization [27, 32], prethermalization [26, 28–31], and dissipation [19, 28] were proposed to slow down the thermalization.

Dissipation has been demonstrated to serve as a resource for performing quantum tasks [33–40]. For instance, by competently designing dissipation to compete with coherent driving [41–48], or by designing competition among dissipative processes including incoherent driving [49], one can achieve dissipative TCs. For the driving that its time-dependent aspect can be eliminated in a suitable rotating frame, would lead to the continuous TC (CTC) characterized by the spontaneous breaking of continuous TTS [50–57]. These dissipative TCs have been experimentally observed in various systems [58–66]. Perfect TC should exhibit infinite lifetime [67–70], representing with a robust neverending oscillatory (OSC). This mathematically corresponds to a stable closed tra-

jectory in phase space, defined as limit cycle (LC), a core element in nonlinear dynamical phenomena [71], such as grid power [72], circadian clocks [73] and quantum synchronization [74–81]. The quest for novel nonequilibrium states and phases [82–107] that include OSC phases [98–108] is a fundamentally important task in physics predating TCs.

To the best of our knowledge, all the systems exhibiting LC or TC behavior are subjected to external driving, whether it be Floquet-driven [9–19], incoherent-driven [49], or driven-dissipation [41–46, 50–66] scenarios. However, external driving not only adds complexity to the real system but also raises concerns about heating. Moreover, the presence of driving makes it difficult to discern the contributions of other factors, such as interaction and dissipation, to the OSC behavior. Therefore, a fundamental question arises: Can a purely dissipative quantum system, one without explicit coherent or incoherent external driving, exhibits OSC behaviors? If so, would these oscillations be TCs? Affirmative answers to these questions would open possibilities in realizing dissipation-induced, heating-immunity TCs.

We address this question by theoretically uncovering the nonequilibrium steady-state phase diagram of a dissipative Heisenberg spin system, specifically one without external driving. We showcase the emergent of LC and chaotic steady-states, supported by spin dynamics and linear stability analysis. We qualify the LC as a CTC by examining its robustness against noisy interactions and dissipation in the thermodynamic limit.

System.— We consider a dissipative interacting system

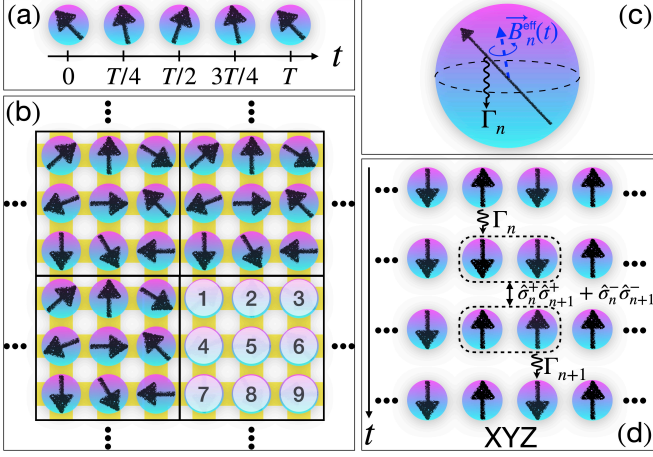


FIG. 1. (a) The periodic oscillation, i.e., CTC. (b) The system paved with infinite 3×3 clusters, each spin is indexed with number $n \in [1, 9]$. (c) Dissipation-induced spin downwards and anisotropic-interaction-induced spin precession. (d) Energy gain and loss mechanism of OSC phases.

described by the Lindblad master equation ($\hbar = 1$),

$$\frac{d\hat{\rho}(t)}{dt} = -i[\hat{H}, \hat{\rho}(t)] + \frac{1}{2} \sum_n \mathcal{D}_n[\hat{\rho}(t)], \quad (1)$$

where \hat{H} is the Hamiltonian governing system's unitary evolution. We consider Hamiltonian as a paradigmatic spin-1/2 Heisenberg XYZ model,

$$\hat{H} = \sum_{\langle mn \rangle} \hat{V}_{mn} = \sum_{\langle mn \rangle} \frac{1}{2d} \sum_{\alpha=x,y,z} J_\alpha \hat{\sigma}_m^\alpha \hat{\sigma}_n^\alpha, \quad (2)$$

where $\hat{\sigma}_n^\alpha$ is the Pauli operator for n th spin and all the spins are localized in a d -dimensional cubic lattice. The nearest-neighbor spin pairs, denoting by $\langle mn \rangle$, are anisotropic interacting with strength J_α . Each spin undergoes an incoherent process of flipping-downward governed by

$$\mathcal{D}_n[\hat{\rho}] = \Gamma (\hat{\sigma}_n^- \hat{\rho} \hat{\sigma}_n^+ - \{\hat{\sigma}_n^+ \hat{\sigma}_n^-, \hat{\rho}\}/2), \quad (3)$$

at strength Γ with $\hat{\sigma}_n^\pm = (\hat{\sigma}_n^x \pm i\hat{\sigma}_n^y)/2$.

These considered single-site dissipations break the time reversibility and other relevant symmetries of system which results in the uniqueness of steady state $\hat{\rho}_{ss} = \lim_{t \rightarrow \infty} \hat{\rho}(t)$ [109–113]. If one state supports a local observable \hat{O} to exhibit infinitely long-lived robust periodic oscillation in the thermodynamic limit, denoted by $\lim_{N \rightarrow \infty} \langle \hat{O} \hat{\rho}_{ss}(t \gg 1) \rangle = O(t)$ with the system size N , which means that the continuous TTS of system is spontaneously broken, giving rise to a CTC [68, 69, 114], as illustrated in Fig. 1(a). This excludes the LC behaviors exhibited by the nonlinear systems with only a few degrees of freedom, such as single van der Pol oscillator [115] and Belousov–Zhabotinsky reactions [116], from being considered as candidates for TCs.

Mean-field phase diagram.— To explore the rich nonequilibrium phases in the thermodynamic limit ($N \rightarrow \infty$) [88], we perform our study at mean-field level which assumes that all spins are uncorrelated, namely the system is in a product state $\hat{\rho} \approx \otimes_{n=1}^{N \rightarrow \infty} \hat{\rho}_n$ [117]. Considering the limitations of the mean field theory in one-dimensional systems [87, 88], we focus on two-dimensional systems paved with infinite 3×3 clusters as shown in Fig. 1(b). In other words, we rewrite density matrix as $\hat{\rho} \approx \hat{\rho}_C \otimes \hat{\rho}_C \otimes \hat{\rho}_C \cdots$ with $\hat{\rho}_C = \otimes_{n=1}^{N_c} \hat{\rho}_n$ and cluster size $N_c = 9$. Therefore, a set of $3N_c$ nonlinear Bloch equations are obtained from Eq. (S2),

$$\begin{aligned} \frac{d\langle \hat{\sigma}_n^x \rangle}{dt} &= -\frac{\Gamma}{2} \langle \hat{\sigma}_n^x \rangle + \sum_m \frac{J_y \langle \hat{\sigma}_n^z \rangle \langle \hat{\sigma}_m^y \rangle - J_z \langle \hat{\sigma}_n^y \rangle \langle \hat{\sigma}_m^z \rangle}{d}, \\ \frac{d\langle \hat{\sigma}_n^y \rangle}{dt} &= -\frac{\Gamma}{2} \langle \hat{\sigma}_n^y \rangle + \sum_m \frac{J_z \langle \hat{\sigma}_n^x \rangle \langle \hat{\sigma}_m^z \rangle - J_x \langle \hat{\sigma}_n^z \rangle \langle \hat{\sigma}_m^x \rangle}{d}, \\ \frac{d\langle \hat{\sigma}_n^z \rangle}{dt} &= -\Gamma (\langle \hat{\sigma}_n^z \rangle + 1) + \sum_m \frac{J_x \langle \hat{\sigma}_n^y \rangle \langle \hat{\sigma}_m^x \rangle - J_y \langle \hat{\sigma}_n^x \rangle \langle \hat{\sigma}_m^y \rangle}{d}, \end{aligned} \quad (4)$$

where n is took within one cluster C and the sum over m encompasses the nearest neighbors of n th spin.

Figure 2(a) shows the phase diagram numerically determined by spin dynamics. The paramagnetic phase aligns all spins down, namely $\langle \hat{\sigma}_n^{x(y)} \rangle = 0, \langle \hat{\sigma}_n^z \rangle = -1$, holding system's Z_2 symmetry ($\hat{\sigma}_n^x \rightarrow -\hat{\sigma}_n^x, \hat{\sigma}_n^y \rightarrow -\hat{\sigma}_n^y$). This Z_2 symmetry of system is spontaneously broken in the ferromagnetic (FM) phase with $\langle \hat{\sigma}_n^{x(y)} \rangle \neq 0$ [118]. The spin-density-wave (SDW) phase has period greater than two lattice sites in at least one direction. In addition to those stationary phases found in [88], a novel nonstationary OSC phase, that spontaneously breaks TTS, emerges inside SDW phase region. Unlike PM and FM, which are spatially uniform phases and can exist without dissipation [88, 119], SDW and OSC are spatially non-uniform state and alive only under nonequilibrium circumstances.

Those OSC phases can be further classified using Lyapunov exponent λ [120]. For example, as shown in Fig. 2(b), we present a detailed phase diagram of OSC phases with fixed $J_y = 1.1$, where the LC and chaos are respectively corresponding to $\lambda = 0$ and $\lambda > 0$ (find more details in [121]). In Fig. 2(c-e), we demonstrate the different dynamical behaviors of SDW, LC, and chaos phases by projecting the dynamic trajectories of magnetization onto the y - z plane of the Bloch sphere. The highlighted circle blocks correspond to the initial states $|\psi_n(t=0)\rangle = (|\uparrow\rangle + e^{i\pi/9}|\downarrow\rangle)/\sqrt{2}$ for the spins with $n = 1, 4, 7$ as labeled in Fig. 1(b). The dynamical behaviors of magnetization $\langle \hat{\sigma}_{n=1,4,7}^{x=y,z} \rangle$ illustrates that the stationary SDW phase corresponds to fixed-points, while either LC attractor or chaotic behavior are observed in the nonstationary OSC phase.

The Heisenberg XXZ model is a loyal supporter of PM, where the system has isotropic interactions ($J_x = J_y$) in

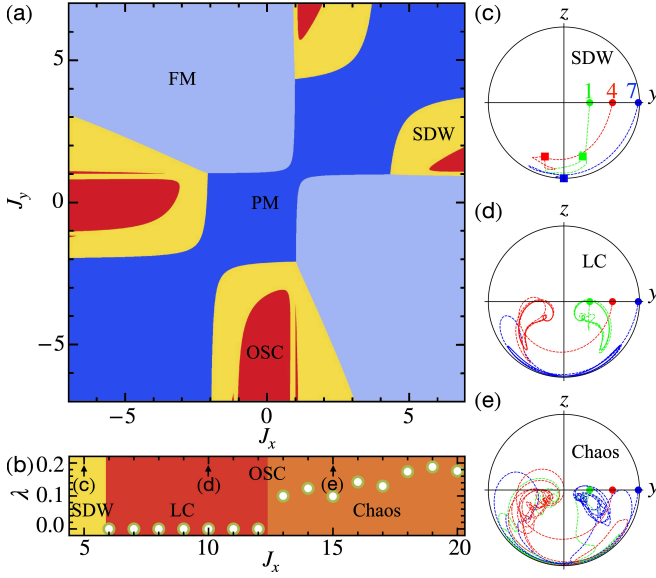


FIG. 2. (a) Nonequilibrium phase diagram with $J_z = \gamma = 1$ (b) Two OSC phases, limit-cycle (LC) and chaos, are distinguished by Lyapunov exponent λ , with $J_y = 1.1$. (c-e) The magnetization dynamic trajectories on y - z plane for spins with $n = 1, 4, 7$. As arrowed in (b), the demonstrated SDW (c), LC (d), and chaos (e) phases correspond to $J_x = 5, 10$ and 15 , respectively. The fixed-point fate of SDW is marked with square blocks.

x - y plane, that conserve magnetization, resulting nothing to counteract the dissipation-induced spin downwards. For XYZ model, anisotropic interaction ($J_x \neq J_y$) breaks the conservation of magnetization, exhibiting spin fluctuation with pairs of spins flipping upwards or downwards simultaneously. This spin fluctuation also allow each spin to precess around its effective magnetic field $\vec{B}_n^{\text{eff}} = \sum_{\langle mn \rangle} (J_x \langle \hat{\sigma}_m^x \rangle, J_y \langle \hat{\sigma}_m^y \rangle, J_z \langle \hat{\sigma}_m^z \rangle)$, originating from interactions with surrounding spins [see Fig. 1(c)]. The competition between the spin fluctuation or precession and the dissipation-induced spin downwards makes the scenario complicated and interesting, leading to the emergent of other novel phases when the dissipation no longer wins. The balanced competition results in the stationary phases such as FM and SDW. This balanced competition would also turn into cooperation under suitable parameters [122], giving rise to energy-conservation-broken nonstationary OSC phases. Figure 1(d) takes the case that neighboring spins tend to align antiparallel, i. e., $J_{\alpha=x,y,z} > 0$ (other cases can be analyzed similarly), to illustrate the microscopic cycle of this dynamical cooperation. The system gains the energy when the dissipation flips down the n th spin [123], following is an energy-conservation process that spin fluctuations cause two neighboring spins be in a coherent superposition of up or down simultaneously. Lastly, when dissipation flips the $(n+1)$ th spin downward to antiparallel with neighboring spins, the system releases energy.

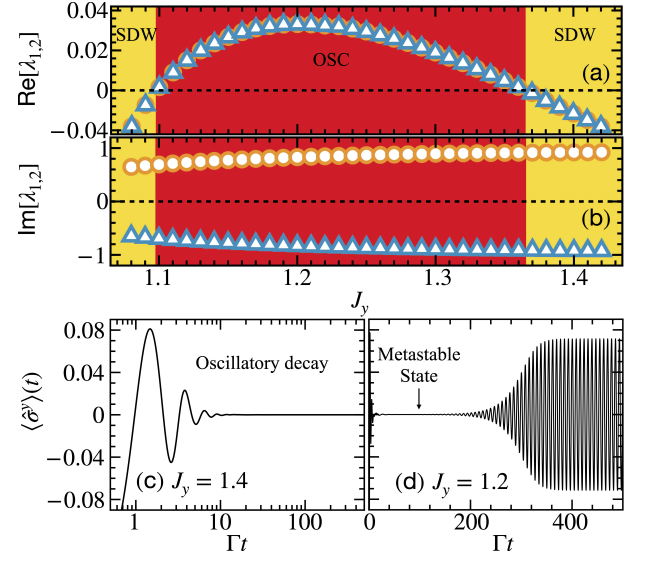


FIG. 3. (a-b) The real and imaginary parts of the first two eigenvalues λ_1 (triangles) and λ_2 (circles) of the Jacobian \mathcal{M} with fixed $J_x = 5.9, J_z = \gamma = 1$. (c-d) The dynamics of $\langle \hat{\sigma}^y \rangle$. The dashed lines highlight zero values. (a-b) share the same x -axis and (c-d) share the same y -axis.

The energy gain and loss of Floquet time crystals primarily came from coherent driving. In driven-dissipative systems, the driven and dissipation can respectively serve as energy gain and loss [41–46, 49–66]. Without driving, if the applied dissipation solely reduces the system’s energy, such as photon leakage from a cavity causing irreversible energy loss, the system would decay to a trivial steady state [58–63]. In our scenario, these microscopic cycles sustain the nonconservative OSC behavior, where dissipation plays both roles of energy gain and loss in cooperation with anisotropic-interaction-induced spin fluctuations. Therefore, our work provides an entirely new mechanism for emerging CTC.

Linear stability analysis.— To further confirm the time-dependent nonequilibrium phase, we introduce the small local perturbations $\delta \hat{\rho}_C$ to the fixed-point solution $\hat{\rho}_C^{(0)}$ of Eq. (S5), which is numerically obtained by setting the left side of Eq. (S5) to zero. The characteristic motion equation for $\delta \hat{\rho}_C$ is derived by linearizing the system and denoted as $\partial_t \delta \hat{\rho}_C = \mathcal{M}[\delta \hat{\rho}_C]$, where the superoperator \mathcal{M} is referred as Jacobian. Therefore, the dynamical behavior of local perturbations can be expressed as $\delta \hat{\rho}_C = \sum_j c_j e^{\lambda_j t} \delta \hat{\rho}_{C,j}$, where c_j and λ_j are respectively the superposition coefficient and eigenvalue corresponding to the j -th eigenmode $\delta \hat{\rho}_{C,j}$ of Jacobian. Here eigenvalues are indexed in descending order of their real parts as $\text{Re}[\lambda_1] \geq \text{Re}[\lambda_2] \geq \dots$. Therefore, when all eigenvalues have negative real parts, $\delta \hat{\rho}_C$ would decay to zero over the system’s relaxation time, indicating that the fixed-point solution $\hat{\rho}_C^{(0)}$ is the steady state. The appearance of eigenvalues with positive real parts results in the expo-

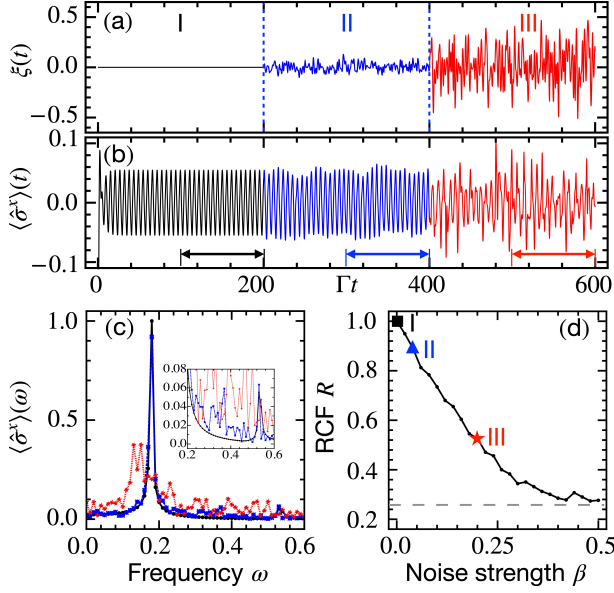


FIG. 4. (a-b) The quiet CTC built without noise (stage I) is perturbed with the segmented weak (stage II) and strong noises (stage III) at $\Gamma t = 200$ and 400 respectively. The noise strengths $\beta_I = 0$, $\beta_{II} = 0.04$, $\beta_{III} = 0.2$ are indicated in (d). (c) shows the Fourier spectrum of the selected arrowed regions in (b), with the zoom-in inset. (d) Relative crystalline fraction R for varying noise strength β . Here the initial state is same as the one used in Fig. 2(c-e), and the undisturbed interaction strengths are $J_x = 7$, $J_y = 1.5$, $J_z = 1$. (a) and (b) share the x -axis.

nentially growth of the local perturbations $\delta\hat{\rho}_C$, reveals that the fixed-point solution $\hat{\rho}_C^{(0)}$ is a metastable state. Interestingly, the system will evolve to a time-dependent steady state if the imaginary parts are nonzero.

Figure 3(a-b) respectively shows the real and imaginary parts of the first two eigenvalues λ_1 (triangles) and λ_2 (circles) of the Jacobian \mathcal{M} . The phase boundaries of the SDW-OSC phases, $J_y = 1.098$ and $J_y = 1.366$, corresponding to the points when the real parts of eigenvalues switch signs, agrees to that in Fig. 2(a). The imaginary parts consistently manifest as non-zero conjugate pairs, suggesting that by selecting an appropriate initial state, the system will: 1) undergo evolution into the time-independent steady state with oscillatory decay behavior in the SDW phase; 2) potentially pass through a metastable state before transitioning into a limit cycle state in the OSC phase. Those behaviors are respectively illustrated in Fig. 3(c-d) by the average magnetization of one cluster, $\langle\hat{\sigma}^{\alpha=x,y,z}\rangle = \sum_{n \in C} \langle\hat{\sigma}_n^{\alpha=x,y,z}\rangle / N_C$ with initial state $|\psi_n(t=0)\rangle = (|\uparrow\rangle + \sqrt{99}e^{i(r_n+c_n)\pi/3}|\downarrow\rangle)/10$, where r_n and c_n denotes the row and column of n th spin.

Rigidity of continuous time crystal.— The rigidity of a CTC requires its periodic OSC behavior exhibits strong robustness against fluctuations of system parameters. Here we consider noisy interactions given by $\tilde{J}_\alpha(t) =$

$J_\alpha + \xi_\beta(t)$, where $\xi_\beta(t)$ represents isotropic Gaussian-type white noise and its standard deviation β acts as intensity. In Fig. 4(a), we design three stages of interactions, the corresponding dynamical behaviors is displayed in Fig. 4(b) with $\langle\hat{\sigma}^x\rangle$, whose Fourier spectrums $\langle\hat{\sigma}^x\rangle(\omega)$ for the selected regions that away from relaxing processes are shown in Fig. 4(c). Without noise (stage I), the system relaxes to a LC-type oscillation, the Fourier spectrum of which features a discernible sharp dominant peak at $\omega = \omega_p = 0.18$ and a tiny peak at $\omega \approx 3\omega_p$, indicating the emergent of a prototypical CTC. Then we perturb the CTC by the weak noise with strength $\beta = 0.04$ at stage II. This perturbation has nearly no effect on the main peak and it only introduces some weak higher-frequency components in Fourier spectrum [see inset of Fig. 4(c)], indicating that the CTC is still thriving. Finally, we quench the system to a much stronger white noise with strength $\beta = 0.2$ at stage III. The regular periodic oscillations are significantly altered and the ω_p component is no longer the prominent principal peak, and numerous other frequency components appear. Consequently, the CTC is softened under this strong noise.

Furthermore, we define the relative crystalline fraction (RCF), $R_\eta = \Omega_\eta / \Omega_I$, to quantify the rigidity of CTC. The crystalline fraction of the stage $\eta = \text{I, II, III}$ is defined as $\Omega_\eta = \sum_{\omega \in [\omega_p - \delta\omega, \omega_p + \delta\omega]} \langle\hat{\sigma}^x\rangle(\omega) / \sum_{\omega \in [0, \Delta\omega]} \langle\hat{\sigma}^x\rangle(\omega)$, with the principal frequency ω_p for quiet case. We take $\delta\omega = 0.08$ and $\Delta\omega = 0.6$ in our calculations. The RCFs for three stages are respectively $R_I = 1$, $R_{II} = 0.89$, and $R_{III} = 0.53$ as remarked in Fig. 4(d), where illustrates how the CTC melts as noise strength increases. The CTC's RCF decreases with increasing noise and stabilizes at the dashed gray line, indicating that even in the presence of strong noise, the system's OSC behavior still may retain some information about the CTC. We also have verified its robustness under other noisy interactions [121] and noisy dissipation.

Experimental realization.— We have recently experimentally implemented independent loss and gain between $|\downarrow\rangle = |F=0, m_F=0\rangle$ and $|\uparrow\rangle = |F=1, m_F=0\rangle$ states in the $^2S_{1/2}$ manifold of $^{171}\text{Yb}^+$. This was achieved by optically pumping the ions to six auxiliary excited states, and then adiabatically eliminating these states that exhibit spontaneous emission [80]. The XYZ interactions have been realized in experiments by coupling the collective motion of ions to the internal states [124–128]. We find that the power-law decay characteristics of these interactions do not affect the existence of OSC behavior [121]. The XYZ interactions have also been proposed to be realizable through techniques such as two-photon resonance in systems like Rydberg atoms, Rydberg-dressed atoms, and dipolar atoms or molecules [88].

Discussions.— We have proposed a CTC mechanism resulting from the competition between dissipation-induced spin downwards and anisotropic-interaction-induced spin precession or spin fluctuation. In the past,

the general understanding of CTCs mainly focused on the interplay of dissipation and driving-induced quantum coherence, but paid less attention to the role of interaction. Thus, this is a completely new ergodic-breaking mechanism in which interactions play a crucial role. Since there is no external drive, the realized CTC is not subject to heating, so its lifetime can be as long as the system's.

This work paves the future explorations of CTCs that is immune to heating in other systems, including Hubbard model [99, 100] and Rydberg model [129–131] using the methods introduced here and other numerical methods [87, 132–135] involving quantum fluctuations and correlations. The experimentally accessible CTC provides further motivation to employ dissipations as resources for exploring nonequilibrium quantum dynamics, like quantum synchronization. The existence of LC and chaotic phases opens a pathway to investigate reversible to irreversible transitions [136] in dissipative quantum systems.

We thank Ran Qi, Qingze Guan, Zhiyuan Sun, Jiansong Pan, Jin Zhang and Weidong Li for valuable discussions. We especially acknowledge Augusto Smerzi for his useful comments and advice on our manuscript. This work was supported by the National Natural Science Foundation of China (Grant No. 12104210, 12088101 and U2330401), the Natural Science Foundation of Top Talent of SZTU (GDRC202202, GDRC202312), and the Guangdong Provincial Quantum Science Strategic Initiative (No. GDZX2305006).

* Corresponding author: lbfu@gscaep.ac.cn

† Corresponding author: Jianwen.Jie1990@gmail.com

- [1] A. Shapere and F. Wilczek, *Phys. Rev. Lett.* **109**, 160402 (2012).
- [2] F. Wilczek, *Phys. Rev. Lett.* **109**, 160401 (2012).
- [3] T. Li, Z.-X. Gong, Z.-Q. Yin, H. T. Quan, X. Yin, P. Zhang, L.-M. Duan, and X. Zhang, *Phys. Rev. Lett.* **109**, 163001 (2012).
- [4] J. Zakrzewski, *Physics* **116** (2012).
- [5] P. Bruno, *Phys. Rev. Lett.* **111**, 070402 (2013).
- [6] P. Nozières, *Europhysics Letters* **103**, 57008 (2013).
- [7] H. Watanabe and M. Oshikawa, *Phys. Rev. Lett.* **114**, 251603 (2015).
- [8] V. K. Kozin and O. Kyriienko, *Phys. Rev. Lett.* **123**, 210602 (2019).
- [9] K. Sacha, *Phys. Rev. A* **91**, 033617 (2015).
- [10] V. Khemani, A. Lazarides, R. Moessner, and S. L. Sondhi, *Phys. Rev. Lett.* **116**, 250401 (2016).
- [11] C. W. von Keyserlingk, V. Khemani, and S. L. Sondhi, *Phys. Rev. B* **94**, 085112 (2016).
- [12] D. V. Else, B. Bauer, and C. Nayak, *Phys. Rev. Lett.* **117**, 090402 (2016).
- [13] N. Y. Yao, A. C. Potter, I.-D. Potirniche, and A. Vishwanath, *Phys. Rev. Lett.* **118**, 030401 (2017).
- [14] P. Richerme, *Physics* **10** (2017).
- [15] A. Russomanno, F. Iemini, M. Dalmonte, and R. Fazio, *Phys. Rev. B* **95**, 214307 (2017).
- [16] F. M. Surace, A. Russomanno, M. Dalmonte, A. Silva, R. Fazio, and F. Iemini, *Phys. Rev. B* **99**, 104303 (2019).
- [17] A. Sakurai, V. M. Bastidas, W. J. Munro, and K. Nemoto, *Phys. Rev. Lett.* **126**, 120606 (2021).
- [18] S. Pal, N. Nishad, T. S. Mahesh, and G. J. Sreejith, *Phys. Rev. Lett.* **120**, 180602 (2018).
- [19] D. V. Else, C. Monroe, C. Nayak, and N. Y. Yao, *Annual Review of Condensed Matter Physics* **11**, 467 (2020).
- [20] P. Xu and T.-S. Deng, *Phys. Rev. B* **107**, 104301 (2023).
- [21] T. Chen, R. Shen, C. H. Lee, B. Yang, and R. W. Bomantara, *arXiv:2309.11560*.
- [22] J. Rovny, R. L. Blum, and S. E. Barrett, *Phys. Rev. Lett.* **120**, 180603 (2018).
- [23] J. Rovny, R. L. Blum, and S. E. Barrett, *Phys. Rev. B* **97**, 184301 (2018).
- [24] S. Choi, J. Choi, R. Landig, G. Kucsko, H. Zhou, J. Isoya, F. Jelezko, S. Onoda, H. Sumiya, V. Khemani, *et al.*, *Nature* **543**, 221 (2017).
- [25] J. Zhang, P. W. Hess, A. Kyprianidis, P. Becker, A. Lee, J. Smith, G. Pagano, I.-D. Potirniche, A. C. Potter, A. Vishwanath, *et al.*, *Nature* **543**, 217 (2017).
- [26] A. Kyprianidis, F. Machado, W. Morong, P. Becker, K. S. Collins, D. V. Else, L. Feng, P. W. Hess, C. Nayak, G. Pagano, N. Y. Yao, and C. Monroe, *Science* **372**, 1192 (2021).
- [27] X. Mi, M. Ippoliti, C. Quintana, A. Greene, Z. Chen, J. Gross, F. Arute, K. Arya, J. Atalaya, R. Babbush, *et al.*, *Nature* **601**, 531 (2022).
- [28] D. V. Else, B. Bauer, and C. Nayak, *Phys. Rev. X* **7**, 011026 (2017).
- [29] T. Mori, *Phys. Rev. B* **98**, 104303 (2018).
- [30] B. Ye, F. Machado, and N. Y. Yao, *Phys. Rev. Lett.* **127**, 140603 (2021).
- [31] A. Pizzi, A. Nunnenkamp, and J. Knolle, *Phys. Rev. Lett.* **127**, 140602 (2021).
- [32] J. Randall, C. E. Bradley, F. V. van der Gronden, A. Galicia, M. H. Abobeih, M. Markham, D. J. Twitchen, F. Machado, N. Y. Yao, and T. H. Taminiau, *Science* **374**, 1474 (2021).
- [33] F. Verstraete, M. M. Wolf, and J. Ignacio Cirac, *Nature physics* **5**, 633 (2009).
- [34] J. F. Poyatos, J. I. Cirac, and P. Zoller, *Phys. Rev. Lett.* **77**, 4728 (1996).
- [35] J. Preskill, *arXiv:2208.08064*.
- [36] Y. Lin, J. Gaebler, F. Reiter, T. R. Tan, R. Bowler, A. Sørensen, D. Leibfried, and D. J. Wineland, *Nature* **504**, 415 (2013).
- [37] S. Shankar, M. Hatridge, Z. Leghtas, K. Sliwa, A. Narla, U. Vool, S. M. Girvin, L. Frunzio, M. Mirrahimi, and M. H. Devoret, *Nature* **504**, 419 (2013).
- [38] P. Magnard, P. Kurpiers, B. Royer, T. Walter, J.-C. Besse, S. Gasparinetti, M. Pechal, J. Heinsoo, S. Storz, A. Blais, and A. Wallraff, *Phys. Rev. Lett.* **121**, 060502 (2018).
- [39] M. Malinowski, C. Zhang, V. Negnevitsky, I. Rojkov, F. Reiter, T.-L. Nguyen, M. Stadler, D. Kienzler, K. K. Mehta, and J. P. Home, *Phys. Rev. Lett.* **128**, 080503 (2022).
- [40] Y. Liu, Z. Wang, C. Yang, J. Jie, and Y. Wang, *Phys. Rev. Lett.* **132**, 216301 (2024).
- [41] Z. Gong and M. Ueda, *Physics* **14** (2021).
- [42] Z. Gong, R. Hamazaki, and M. Ueda, *Phys. Rev. Lett.*

- 120**, 040404 (2018).
- [43] B. Zhu, J. Marino, N. Y. Yao, M. D. Lukin, and E. A. Demler, *New Journal of Physics* **21**, 073028 (2019).
- [44] A. Lazarides, S. Roy, F. Piazza, and R. Moessner, *Phys. Rev. Res.* **2**, 022002(R) (2020).
- [45] A. Riera-Campen, M. Moreno-Cardoner, and A. Sanpera, *Quantum* **4**, 270 (2020).
- [46] A. Sakurai, V. M. Bastidas, M. P. Estarellas, W. J. Munro, and K. Nemoto, *Phys. Rev. B* **104**, 054304 (2021).
- [47] B. Berislav and J. Dieter, *Phys. Rev. Lett.* **123**, 260401 (2019).
- [48] B. Berislav, T. Joseph, and J. Dieter, *Nature Communications* **10**, 1730 (2019).
- [49] F. Minganti, I. I. Arkhipov, A. Miranowicz, and F. Nori, *arXiv:2008.08075*.
- [50] M. Hajdušek, P. Solanki, R. Fazio, and S. Vinjanampathy, *Phys. Rev. Lett.* **128**, 080603 (2022).
- [51] M. Krishna, P. Solanki, M. Hajdušek, and S. Vinjanampathy, *Phys. Rev. Lett.* **130**, 150401 (2023).
- [52] H. Keßler, J. G. Cosme, M. Hemmerling, L. Mathey, and A. Hemmerich, *Phys. Rev. A* **99**, 053605 (2019).
- [53] K. Tucker, B. Zhu, R. J. Lewis-Swan, J. Marino, F. Jimenez, J. G. Restrepo, and A. M. Rey, *New Journal of Physics* **20**, 123003 (2018).
- [54] C. Lledó, T. K. Mavrogordatos, and M. H. Szymańska, *Phys. Rev. B* **100**, 054303 (2019).
- [55] K. Seibold, R. Rota, and V. Savona, *Phys. Rev. A* **101**, 033839 (2020).
- [56] L. F. d. Prazeres, L. d. S. Souza, and F. Iemini, *Phys. Rev. B* **103**, 184308 (2021).
- [57] F. Iemini, A. Russomanno, J. Keeling, M. Schirò, M. Dalmonte, and R. Fazio, *Phys. Rev. Lett.* **121**, 035301 (2018).
- [58] H. Keßler, P. Kongkhambut, C. Georges, L. Mathey, J. G. Cosme, and A. Hemmerich, *Phys. Rev. Lett.* **127**, 043602 (2021).
- [59] P. Kongkhambut, H. Keßler, J. Skulte, L. Mathey, J. G. Cosme, and A. Hemmerich, *Phys. Rev. Lett.* **127**, 253601 (2021).
- [60] P. Kongkhambut, J. Skulte, L. Mathey, J. G. Cosme, A. Hemmerich, and H. Keßler, *Science* **377**, 670 (2022).
- [61] N. Dogra, M. Landini, K. Kroeger, L. Hruby, T. Donner, and T. Esslinger, *Science* **366**, 1496 (2019).
- [62] P. Zupancic, D. Dreon, X. Li, A. Baumgärtner, A. Morales, W. Zheng, N. R. Cooper, T. Esslinger, and T. Donner, *Phys. Rev. Lett.* **123**, 233601 (2019).
- [63] D. Dreon, A. Baumgärtner, X. Li, S. Hertlein, T. Esslinger, and T. Donner, *Nature* **608**, 494 (2022).
- [64] H. Taheri, A. B. Matsko, L. Maleki, and K. Sacha, *Nature communications* **13**, 848 (2022).
- [65] S. Autti, V. B. Eltsov, and G. E. Volovik, *Phys. Rev. Lett.* **120**, 215301 (2018).
- [66] A. J. E. Kreil, H. Y. Musienko-Shmarova, S. Eggert, A. A. Serga, B. Hillebrands, D. A. Bozhko, A. Pomyalov, and V. S. L'vov, *Phys. Rev. B* **100**, 020406(R) (2019).
- [67] K. Sacha and J. Zakrzewski, *Reports on Progress in Physics* **81**, 016401 (2017).
- [68] V. Khemani, R. Moessner, and S. L. Sondhi, *arXiv:1910.10745 [cond-mat.str-el]*.
- [69] M. P. Zaletel, M. Lukin, C. Monroe, C. Nayak, F. Wilczek, and N. Y. Yao, *Rev. Mod. Phys.* **95**, 031001 (2023).
- [70] L. Guo and P. Liang, *New Journal of Physics* **22**, 075003 (2020).
- [71] S. Strogatz, *Nonlinear Dynamics and Chaos: With Applications to Physics, Biology, Chemistry, and Engineering* (CRC Press, 2018).
- [72] A. Kasis, N. Monshizadeh, and I. Lestas, *Automatica* **131**, 109736 (2021).
- [73] D. Gonze, *Open Life Sciences* **6**, 712 (2011).
- [74] N. Lörch, S. E. Nigg, A. Nunnenkamp, R. P. Tiwari, and C. Bruder, *Phys. Rev. Lett.* **118**, 243602 (2017).
- [75] S. E. Nigg, *Phys. Rev. A* **97**, 013811 (2018).
- [76] A. Roulet and C. Bruder, *Phys. Rev. Lett.* **121**, 053601 (2018).
- [77] M. Koppenhöfer and A. Roulet, *Phys. Rev. A* **99**, 043804 (2019).
- [78] A. W. Laskar, P. Adhikary, S. Mondal, P. Katiyar, S. Vinjanampathy, and S. Ghosh, *Phys. Rev. Lett.* **125**, 013601 (2020).
- [79] A. Parra-López and J. Bergli, *Phys. Rev. A* **101**, 062104 (2020).
- [80] L. Zhang, Z. Wang, Y. Wang, J. Zhang, Z. Wu, J. Jie, and Y. Lu, *Phys. Rev. Res.* **5**, 033209 (2023).
- [81] Z. Wang, R. Qi, Y. Lu, Z. Wu, and J. Jie, *arXiv:2302.00976*.
- [82] X. Nie and W. Zheng, *Phys. Rev. A* **107**, 033311 (2023).
- [83] H. Breuer, F. Petruccione, and S. Petruccione, *The Theory of Open Quantum Systems* (Oxford University Press, 2002).
- [84] Á. Rivas and S. Huelga, *Open Quantum Systems: An Introduction*, SpringerBriefs in Physics (Springer Berlin Heidelberg, 2011).
- [85] I. de Vega and D. Alonso, *Rev. Mod. Phys.* **89**, 015001 (2017).
- [86] H. Weimer, A. Kshetrimayum, and R. Orús, *Rev. Mod. Phys.* **93**, 015008 (2021).
- [87] J. Jin, A. Biella, O. Viyuela, L. Mazza, J. Keeling, R. Fazio, and D. Rossini, *Phys. Rev. X* **6**, 031011 (2016).
- [88] T. E. Lee, S. Gopalakrishnan, and M. D. Lukin, *Phys. Rev. Lett.* **110**, 257204 (2013).
- [89] J. Jin, D. Rossini, R. Fazio, M. Leib, and M. J. Hartmann, *Phys. Rev. Lett.* **110**, 163605 (2013).
- [90] A. Le Boité, G. Orso, and C. Ciuti, *Phys. Rev. Lett.* **110**, 233601 (2013).
- [91] M. Fitzpatrick, N. M. Sundaresan, A. C. Y. Li, J. Koch, and A. A. Houck, *Phys. Rev. X* **7**, 011016 (2017).
- [92] L. Song and J. Jin, *Phys. Rev. B* **108**, 054302 (2023).
- [93] Y. Zhang and T. Barthel, *Phys. Rev. Lett.* **129**, 120401 (2022).
- [94] Z. Li, F. Claude, T. Boulier, E. Giacobino, Q. Glorieux, A. Bramati, and C. Ciuti, *Phys. Rev. Lett.* **128**, 093601 (2022).
- [95] J. Kazemi and H. Weimer, *Phys. Rev. Lett.* **130**, 163601 (2023).
- [96] Y. Li, X. Li, and J. Jin, *Phys. Rev. A* **107**, 042205 (2023).
- [97] T. Haga, *Phys. Rev. A* **107**, 052208 (2023).
- [98] T. E. Lee, H. Häffner, and M. C. Cross, *Phys. Rev. A* **84**, 031402(R) (2011).
- [99] R. M. Wilson, K. W. Mahmud, A. Hu, A. V. Gorshkov, M. Hafezi, and M. Foss-Feig, *Phys. Rev. A* **94**, 033801 (2016).
- [100] M. Schiró, C. Joshi, M. Bordyuh, R. Fazio, J. Keeling,

- and H. E. Türeci, *Phys. Rev. Lett.* **116**, 143603 (2016).
- [101] C. D. Parmee and N. R. Cooper, *Phys. Rev. A* **97**, 053616 (2018).
- [102] C. D. Parmee and N. R. Cooper, *Journal of Physics B: Atomic, Molecular and Optical Physics* **53**, 135302 (2020).
- [103] J. Qian, G. Dong, L. Zhou, and W. Zhang, *Phys. Rev. A* **85**, 065401 (2012).
- [104] E. T. Owen, J. Jin, D. Rossini, R. Fazio, and M. J. Hartmann, *New Journal of Physics* **20**, 045004 (2018).
- [105] C.-K. Chan, T. E. Lee, and S. Gopalakrishnan, *Phys. Rev. A* **91**, 051601(R) (2015).
- [106] X. Li, Y. Li, and J. Jin, *Phys. Rev. A* **107**, 032219 (2023).
- [107] G. Passarelli, P. Lucignano, R. Fazio, and A. Russo-manno, *Phys. Rev. B* **106**, 224308 (2022).
- [108] Y. M. Bunkov and G. E. Volovik, [arXiv:1003.4889](https://arxiv.org/abs/1003.4889).
- [109] D. E. Evans, *Commun.Math. Phys.* **54**, 293 (1977).
- [110] A. Frigerio, *Communications in Mathematical Physics* **63**, 269 (1978).
- [111] T. Prosen, *Physica Scripta* **86**, 058511 (2012).
- [112] T. Prosen, *Journal of Physics A: Mathematical and Theoretical* **48**, 373001 (2015).
- [113] S. G. Schirmer and X. Wang, *Phys. Rev. A* **81**, 062306 (2010).
- [114] V. Khemani, C. W. von Keyserlingk, and S. L. Sondhi, *Phys. Rev. B* **96**, 115127 (2017).
- [115] A. Pikovsky, J. Kurths, M. Rosenblum, J. Kurths, B. Chirikov, C. U. Press, P. Cvitanovic, F. Moss, and H. Swinney, *Synchronization: A Universal Concept in Nonlinear Sciences*, Cambridge Nonlinear Science Series (Cambridge University Press, 2001).
- [116] R. Enns and G. McGuire, *Nonlinear Physics with Maple for Scientists and Engineers* (Birkhäuser Boston, 2012).
- [117] We conduct precise full quantum numerical calculations on finite-size systems under periodic boundary conditions and find that the two-body correlations weaken gradually as the system size increases. This observation is consistent with approximate treatments in mean-field methods, find more details in the supplementary material ().
- [118] The antiferromagnetic (AFM) and staggering XY (sXY) phases found in [88] would emerge when the selected cluster contains even number of spins along any axis. See more details in Sec. V of the supplementary material ().
- [119] S. Sachdev, *Quantum Phase Transitions*, 2nd ed. (Cambridge University Press, 2011).
- [120] I. I. Yusipov, O. S. Vershinina, S. Denisov, S. P. Kuznetsov, and M. V. Ivanchenko, *Chaos: An Interdisciplinary Journal of Nonlinear Science* **29**, 063130 (2019).
- [121] See Supplemental Material for details on (I) Calculation of Lyapunov exponent; (II) The robustness of CTC under $1/f$ noise; (III) Two body quantum correlations in finite-sized systems; (IV) The oscillatory behavior under power-law decay interaction; (V) Nonequilibrium phase diagram of the systems cluster sizes 2×2 and 4×4 .
- [122] Nontrivial ordered states are achievable only with sufficiently strong anisotropic interaction. Therefore, the considered parameter range must be large enough. Furthermore, for SDW and OSC, the number of spin greater than two is required in at least one direction within a cluster. Thus assuming a sufficiently large cluster size is crucial for obtaining a broader range of possible states ().
- [123] This process also would be recognized as implicit incoherent drive in the sense that it helps system to gain the energy ().
- [124] S. Debnath, N. M. Linke, C. Figgatt, K. A. Landsman, K. Wright, and C. Monroe, *Nature* **536**, 63 (2016).
- [125] F. Kranzl, S. Birnkammer, M. K. Joshi, A. Bastianello, R. Blatt, M. Knap, and C. F. Roos, *Phys. Rev. X* **13**, 031017 (2023).
- [126] Y. Lu, S. Zhang, K. Zhang, W. Chen, Y. Shen, J. Zhang, J.-N. Zhang, and K. Kim, *Nature* **572**, 363 (2019).
- [127] C. Monroe, W. C. Campbell, L.-M. Duan, Z.-X. Gong, A. V. Gorshkov, P. W. Hess, R. Islam, K. Kim, N. M. Linke, G. Pagano, P. Richerme, C. Senko, and N. Y. Yao, *Rev. Mod. Phys.* **93**, 025001 (2021).
- [128] J. Zhang, G. Pagano, P. W. Hess, A. Kyprianidis, P. Becker, H. Kaplan, A. V. Gorshkov, Z.-X. Gong, and C. Monroe, *Nature* **551**, 601 (2017).
- [129] C. Nill, K. Brandner, B. Olmos, F. Carollo, and I. Lesanovsky, *Phys. Rev. Lett.* **129**, 243202 (2022).
- [130] J. Kazemi and H. Weimer, *Phys. Rev. Lett.* **130**, 163601 (2023).
- [131] F. M. Gambetta, F. Carollo, M. Marcuzzi, J. P. Garrahan, and I. Lesanovsky, *Phys. Rev. Lett.* **122**, 015701 (2019).
- [132] U. Schollwöck, *Rev. Mod. Phys.* **77**, 259 (2005).
- [133] J. Cui, J. I. Cirac, and M. C. Bañuls, *Phys. Rev. Lett.* **114**, 220601 (2015).
- [134] R. Rota, F. Minganti, C. Ciuti, and V. Savona, *Phys. Rev. Lett.* **122**, 110405 (2019).
- [135] S. Finazzi, A. Le Boité, F. Storme, A. Baksic, and C. Ciuti, *Phys. Rev. Lett.* **115**, 080604 (2015).
- [136] C. Reichardt, I. Regev, K. Dahmen, S. Okuma, and C. J. O. Reichardt, [arXiv:2211.03775](https://arxiv.org/abs/2211.03775).

I. CALCULATION OF LYAPUNOV EXPONENT

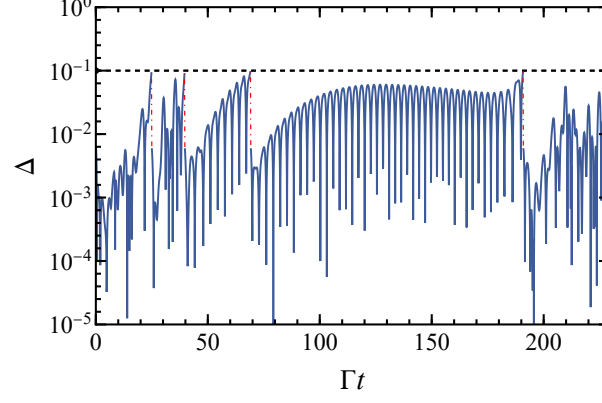


FIG. S1. (color online) Time evolution of the distance $\Delta(t)$ between the fiducial trajectory and auxiliary trajectory for chaotic phase. The black dashed horizontal line denotes the given threshold $\Delta_{\max} = 0.1$ for resetting the auxiliary trajectory (red dot-dashed vertical lines). Here $J_x = 13$, $J_y = 1.1$, $J_z = \gamma = 1.0$.

We employ the largest Lyapunov exponent (LE), a metric introduced in [120], to make discrimination between a limit cycle and chaos behavior. In analogy to the classical definition, we use two quantum trajectories, fiducial trajectory and auxiliary trajectory, to simulate the evolution of the system. Here the auxiliary trajectory is initialized as a normalized state but with a perturbation on the normalized initial fiducial state $\psi_f^{\text{ini.}}$, namely $\psi_a^{\text{ini.}} = \psi_f^{\text{ini.}} + \varepsilon \psi_{\text{ran.}}$ with the random perturbative state $\psi_{\text{ran.}}$ and $\varepsilon \ll 1$. The definition of the largest LE is based on the distance of these two trajectories and the distance is defined as difference between observables of these two trajectories. Here we choose the magnetization along y direction $\bar{\sigma}^y(t) = \frac{1}{N_C} \sum_{n \in C} \langle \psi_n(t) | \hat{\sigma}^y(t) | \psi_n(t) \rangle$ as the observable. The initial distance $\Delta(t=0) = |\bar{\sigma}_f^y(t=0) - \bar{\sigma}_a^y(t=0)|$ plays the reference during the time evolution. When the time-dependent distance $\Delta(t) = |\bar{\sigma}_f^y(t) - \bar{\sigma}_a^y(t)|$ exceeds a given threshold Δ_{\max} at a time t_k , $\Delta(t_k)$ is reset to the initial distance $\Delta(t=0)$ through renormalizing the auxiliary trajectory close to the fiducial trajectory. Finally, the largest LE is given by

$$\lambda = \lim_{t \rightarrow \infty} \frac{1}{t} \sum_k \ln d_k, \quad (\text{S1})$$

where k indexes each time point that the threshold Δ_{\max} is touched and $d_k = \Delta(t_k)/\Delta_0$. The fact that auxiliary trajectory respectively tends to being attracted to the fiducial state in the limit cycle case and tends to away from the fiducial state in the chaos behavior, results in vanished LE $\lambda = 0$ and nonzero LE $\lambda \neq 0$ for limit cycle and chaos behavior respectively.

As shown in Fig. S1, here we consider the parameters as $J_x = 13$, $J_y = 1.1$, $J_z = \gamma = 1.0$, corresponding to the chaotic phase in the Figure 2(b) of the main text. It can be observed that the dynamical distance Δ frequently touches the set threshold distance Δ_{\max} during the evolution, indicating the non-zero LE $\lambda = 0.1$ for the corresponding chaotic scenario.

II. THE ROBUSTNESS OF CTC UNDER $1/f$ NOISE

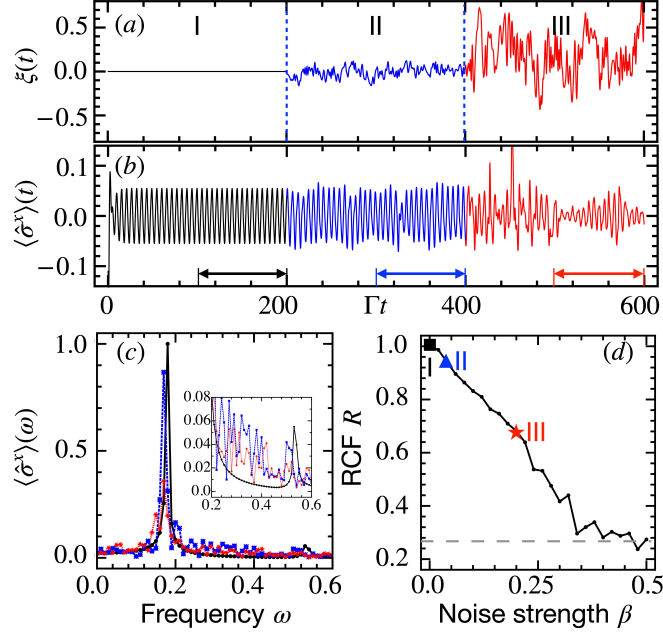


FIG. S2. (color online) The robustness against $1/f$ noise in interactions. (a-b) The CTC built without noise (stage I) is perturbed with the segmented weak (stage II) and strong noises (stage III) at $\Gamma t = 200$ and 400 respectively. The noise strengths $\beta_I = 0$, $\beta_{II} = 0.04$, $\beta_{III} = 0.2$ are indicated in (d). (c) shows the Fourier spectrum of the selected arrowed regions in (b), with the zoom-in inset. (d) Relative crystalline fraction R for varying noise strength β . Here the initial state is same as the one used in Fig. 2(c-e), and the undisturbed interaction strengths are $J_x = 7$, $J_y = 1.5$, $J_z = 1$. (a) and (b) share the x -axis.

$1/f$ noise, often referred to as flicker noise or pink noise, represents a specific type of noise marked by a frequency spectrum that diminishes with increasing frequency. To clarify, the power spectral density of $1/f$ noise follows an inverse proportionality to the frequency, resulting in a higher concentration of power at lower frequencies. Here we consider the robustness of CTC under $1/f$ noise. The noisy interaction is given by $\tilde{J}_\alpha(t) = J_\alpha + \xi_\beta(t)$, where $\xi_\beta(t)$ represents $1/f$ noise and its standard deviation β acts as intensity.

Similar to the consideration of isotropic Gaussian-type white noise shown in Fig. 4 in the main text, here we show the results in Fig. S2. Three stages of time-dependent interactions with $1/f$ noise are shown in Fig. S2(a) and the corresponding dynamical behaviors is displayed in Fig. S2(b) with $\langle \hat{\sigma}^x \rangle$, whose Fourier spectrums for the selected regions that away from relaxing processes are shown in Fig. S2(c). Without noise (stage I), the system relaxes to a LC-type oscillation, the Fourier spectrum of which features a discernible sharp dominant peak at $\omega = \omega_p = 0.18$ and a tiny peak at $\omega \approx 3\omega_p$, indicating the emergent of a prototypical CTC. Then we perturb the CTC by introducing the weak $1/f$ noise with strength $\beta = 0.04$ at $\Gamma t = 200$ (stage II), this perturbation slightly shift the dominant peak to the low frequency regime and introduces some weak higher-frequency components into the OSC behavior as illustrated in the inset of Fig. S2(c), indicating that the CTC is still well alive. Finally, we quench the $1/f$ noise to a much stronger one with strength $\beta = 0.2$ at $\Gamma t = 400$ (stage III), which significantly alters the regular periodic oscillations. Interestingly, Although the amplitudes of the oscillating is changed significantly, but the prominent principal peak of frequency spectrum is not shifted a lot. Figure S2(d) shows the relative crystalline fraction (RCF). The RCFs for three stages are respectively $R_I = 1$, $R_{II} = 0.94$, and $R_{III} = 0.68$ as remarked in Fig. S2(d), where illustrates how the CTC melts as noise strength increases. The CTC's RCF decreases with increasing noise and stabilizes at the dashed gray line, indicating that even in the presence of strong noise, the system's OSC behavior still may retain some information about the CTC.

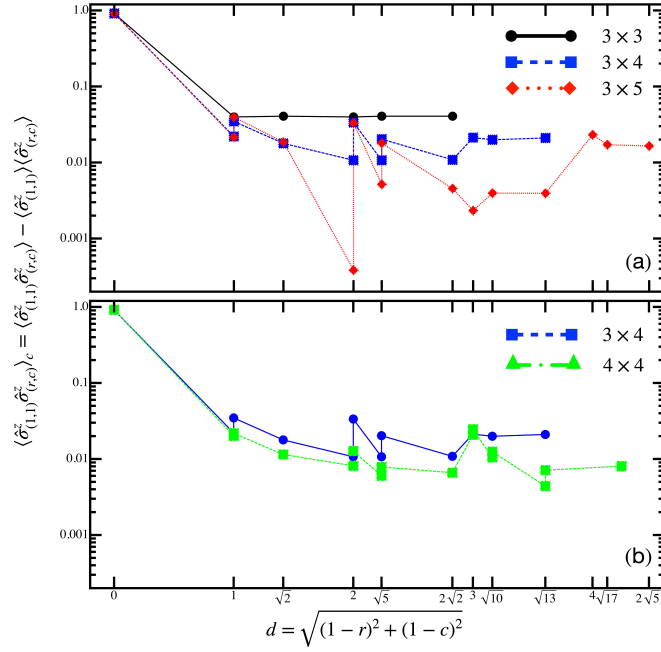


FIG. S3. Two-body correlations are shown for different finite-size 2D systems. (a) compares systems of sizes 3×3 , 3×4 , and 3×5 , while (b) compares systems of sizes 3×4 and 4×4 . Both panels share the same labels for the x-axis and y-axis. The notation (r, c) denotes the position of a spin located at the r -th row and c -th column. The interaction parameters are set to $J_x = 5.9$, $J_y = 1.2$, $J_z = \gamma = 1.0$.

III. TWO BODY QUANTUM CORRELATIONS IN FINITE-SIZED SYSTEMS

In our mean-field calculations, all spins are assumed to form the entire system in a product state, so correlations between spins are not considered. Typically, directly considering quantum correlations in the thermodynamic limit is challenging. To explore the correlations in our system, we start by examining the two-body correlations in a finite-size system and study how these correlations change as the system size increases.

Specifically, we consider the parameters in the OSC region of Fig. 2a in the main text, denoted as $J_x = 5.9$, $J_y = 1.2$, $J_z = \gamma = 1.0$. We examine the two-body spin-spin correlations along z axis, $\langle \hat{\sigma}_j^z \hat{\sigma}_k^z \rangle_c = \langle \hat{\sigma}_j^z \hat{\sigma}_k^z \rangle - \langle \hat{\sigma}_j^z \rangle \langle \hat{\sigma}_k^z \rangle$. When $\langle \hat{\sigma}_j^z \hat{\sigma}_k^z \rangle_c \neq 0$, there are correlations between spins. For this finite-size system, we use a fully quantum method to solve the Lindblad equation shown in Eq. (1) of the main text, and obtain the results shown in Fig. S3.

As shown in Fig. S3, we computed the steady states of two-dimensional systems with sizes 3×3 , 3×4 , 3×5 , and 4×4 under periodic boundary conditions. We then calculated the two-body correlation between the first spin (located at the first row and first column) and other spins. In Fig. S3(a), we compare the results of the 3×3 , 3×4 , and 3×5 systems; and in Fig. S3(b), we compare the results of the 3×4 and 4×4 systems. The numerical results of both comparison groups indicate that as the size of the finite system increases, the two-body correlations gradually weaken. This suggests that in the thermodynamic limit, the two-body correlations will not play the key role. This prediction aligns with the approximations made in our mean-field method.

IV. THE OSCILLATORY BEHAVIOR UNDER POWER-LAW DECAY INTERACTION

In current trapped-ion platform [124–127], it is possible to achieve Heisenberg XYZ interactions. However, these interactions are power-law decay with distance, whereas the interactions discussed in our work are primarily nearest-neighbor XYZ interactions. For the dissipation of spin-1/2 particles or qubits, well-established optical pumping methods can already achieve this. In our recent trapped-ion experimental work [80], we successfully realized a pair of independent dissipations, one is the decay process that spin jumps from $|\uparrow\rangle$ to $|\downarrow\rangle$ and another one is the gain process that spin jumps from $|\downarrow\rangle$ to $|\uparrow\rangle$, by optically pumping the ion from the targeted two lower energy levels to the six auxiliary excited energy levels.

Although the interaction realized in trapped-ion are power-law decay with distance, our calculations show that even

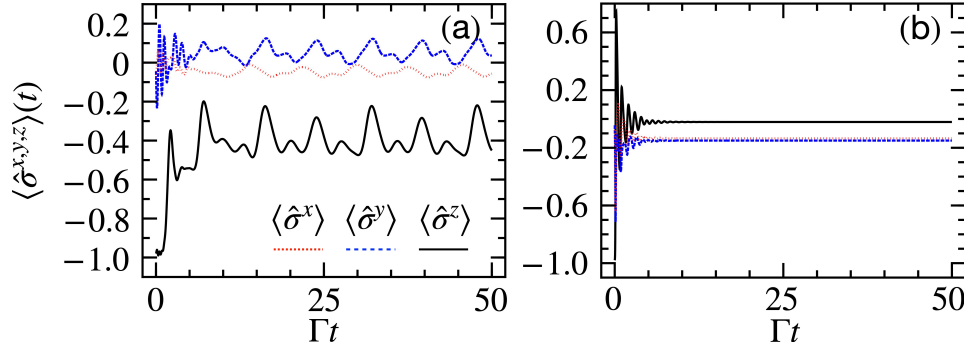


FIG. S4. The dynamics of $\langle \hat{\sigma}^{x,y,z} \rangle$ for the dissipated Heisenberg spin systems with power law decay XYZ interaction. The parameters are set to $J_y = 9$, $J_z = \gamma = 1$, $\beta = 1$. Panels (a) and (b) show the OSC-type steady state ($J_x = 0$) and non-OSC-type steady state ($J_x = 9$), respectively. The initial state is the same as the one used in the Fig. 3(b-c) of the main text. Both panels share the same y-axis label.

this type of power law decaying interaction can induce oscillatory behavior as illustrated in Fig. S4. To obtain those results, we start with setting the following Lindblad equation,

$$\frac{d\hat{\rho}(t)}{dt} = -i [\hat{H}, \hat{\rho}(t)] + \frac{1}{2} \sum_n \mathcal{D}_n[\hat{\rho}(t)], \quad (\text{S2})$$

with the dissipation

$$\mathcal{D}_n[\hat{\rho}] = \Gamma (\hat{\sigma}_n^- \hat{\rho} \hat{\sigma}_n^+ - \{\hat{\sigma}_n^+ \hat{\sigma}_n^-, \hat{\rho}\}/2), \quad (\text{S3})$$

and the Hamiltonian

$$\hat{H} = \frac{1}{2d} \sum_{m,n} \sum_{\alpha=x,y,z} \frac{J_\alpha}{|r_m - r_n|^\beta} \hat{\sigma}_m^\alpha \hat{\sigma}_n^\alpha, \quad (\text{S4})$$

where $r_{m(n)}$ is the position of $m(n)$ th spin and the exponent β determines the range of the interaction can be set to $0 < \beta < 3$ by adjusting the laser detunings [124–127]. Applying the mean-field method used in our work, we obtain the following a set of $3N_c$ coupled nonlinear Bloch equations

$$\frac{d\langle \hat{\sigma}_n^x \rangle}{dt} = -\frac{\Gamma}{2} \langle \hat{\sigma}_n^x \rangle + \frac{1}{d} \sum_{m \neq n} \frac{J_y \langle \hat{\sigma}_n^z \rangle \langle \hat{\sigma}_m^y \rangle - J_z \langle \hat{\sigma}_n^y \rangle \langle \hat{\sigma}_m^z \rangle}{|r_m - r_n|^\beta}, \quad (\text{S5})$$

$$\frac{d\langle \hat{\sigma}_n^y \rangle}{dt} = -\frac{\Gamma}{2} \langle \hat{\sigma}_n^y \rangle + \frac{1}{d} \sum_{m \neq n} \frac{J_z \langle \hat{\sigma}_n^x \rangle \langle \hat{\sigma}_m^z \rangle - J_x \langle \hat{\sigma}_n^z \rangle \langle \hat{\sigma}_m^x \rangle}{|r_m - r_n|^\beta}, \quad (\text{S6})$$

$$\frac{d\langle \hat{\sigma}_n^z \rangle}{dt} = -\Gamma (\langle \hat{\sigma}_n^z \rangle + 1) + \frac{1}{d} \sum_{m \neq n} \frac{J_x \langle \hat{\sigma}_n^y \rangle \langle \hat{\sigma}_m^x \rangle - J_y \langle \hat{\sigma}_n^x \rangle \langle \hat{\sigma}_m^y \rangle}{|r_m - r_n|^\beta}. \quad (\text{S7})$$

Thus, the results in Fig. S4 can be obtained by numerically solving the above coupled nonlinear Bloch equations. In Fig. S4, we set $\beta = 1$, $J_y = 9$, $J_z = \gamma = 1$ and use the initial state from Fig. 3(b-c) in the main text. We find that OSC oscillations occur when the interaction is anisotropic (Fig. S4(a), $J_x = 0 \neq J_y$). However, for isotropic interactions (Fig. S4(b), $J_x = J_y = 9$), the system evolves to a non-OSC steady state. Therefore, we believe that the current trapped-ion platform already have the experimental conditions necessary to observe nonequilibrium oscillatory behavior.

V. NONEQUILIBRIUM PHASE DIAGRAM OF THE SYSTEMS CLUSTER SIZES 2×2 AND 4×4

In our mean-field method, the system is assumed to be filled with identical clusters repeated throughout. Therefore, the symmetrical structure of a single cluster constrains the possible nonequilibrium steady states that can be achieved. For clusters of even length, such as $N_c = 2$, an antiferromagnetic configuration can be constructed. However, for

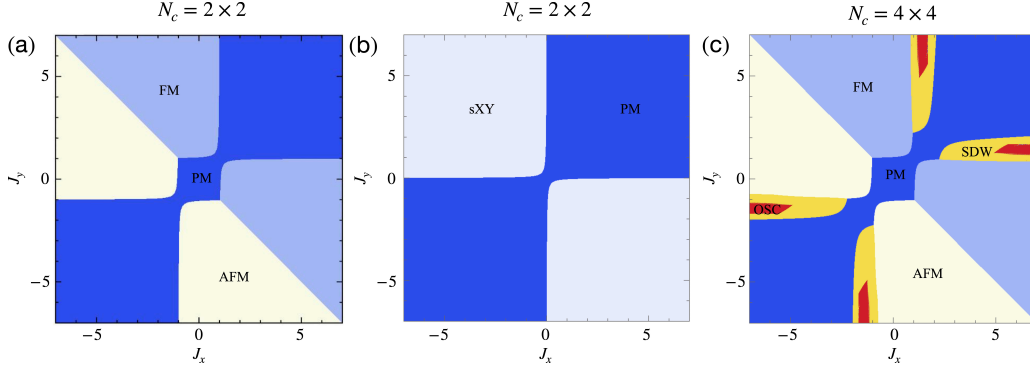


FIG. S5. Nonequilibrium phase diagram for the cluster sizes 2×2 with $J_z = 1$ (a), 2×2 with $J_z = 0$ (b), and 4×4 (c) with $J_z = \gamma = 1$.

clusters of odd length, such as $N_c = 3$, an antiferromagnetic configuration cannot be constructed. These analyses also apply to the spatial configuration of a staggering XY phase with an even period. The results shown in Fig. 2(a) in the main text are for the 3×3 cluster; hence, the antiferromagnetic and staggering XY phases mentioned in [88] cannot be constructed.

As illustrated in Fig. S5(a-b), when we set the cluster size to 2×2 , both the antiferromagnetic and staggering XY phases appear at $J_z = 1$ [Fig. S5(a)] and $J_z = 0$ [Fig. S5(b)], respectively. Fig. S5(a) clearly shows that a 2×2 cluster cannot realize the SDW phase as described in [88] which is consistent with the definition of SDW requiring a spin repetition period of greater than 2 in at least one direction. Fig. S5(c) shows the results for a 4×4 cluster, where, in addition to the phases observed in Fig. 2(a) in the main text, the antiferromagnetic phase also appears.